# Magnetic labeling of primary murine monocytes using very small superparamagnetic iron oxide nanoparticles

Martin Pohland[1], Christoph Pohland[1], Jürgen Kiwit[2], Jana Glumm[1, 2, *]

## From the Contents

**Graphical Abstract** *Very small superparamagnetic iron oxide nanoparticles do not affect the homeostasis of blood-derived monocytes: assessment of viability, cytokine & chemokine secretion, as well as iron uptake*
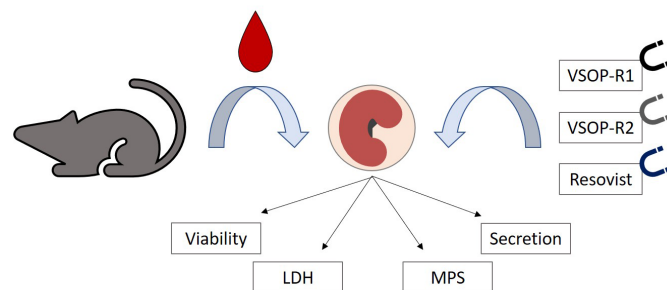
## Abstract

Due to their very small size, nanoparticles can interact with all cells in the central nervous system. One of the most promising nanoparticle subgroups are very small superparamagnetic iron oxide nanoparticles (VSOP) that are citrate coated for electrostatic stabilization. To determine their influence on murine blood-derived monocytes, which easily enter the injured central nervous system, we applied VSOP and carboxydextran-coated superparamagnetic iron oxide nanoparticles (Resovist). We assessed their impact on the viability, cytokine, and chemokine secretion, as well as iron uptake of murine blood-derived monocytes. We found that (1) the monocytes accumulated VSOP and Resovist, (2) this uptake seemed to be nanoparticle- and time-dependent, (3) the decrease of monocytes viability was treatment-related, (4) VSOP and Resovist incubation did not alter cytokine homeostasis, and (5) overall a 6-hour treatment with 0.75 mM VSOP-R1 was probably sufficient to effectively label monocytes for future experiments. Since homeostasis is not altered, it is safe to label blood-derived monocles with VSOP. VSOP labeled monocytes can be used to study injured central nervous system sites further, for example with drug-carrying VSOP.
**Key Words:** CD11b, cytokine; Ferucarbotran; Mac1; MPS; MRI; Resovist; superparamagnetic iron oxide nanoparticles (SPIO); very small superparamagnetic iron oxide nanoparticles (VSOP); viability

## Introduction

From the initial graft experiments (Billingham and Boswell, 1953) to the current rediscovery of the central nervous system (CNS) lymphatic vessels (Louveau et al., 2015b), the peculiarity of the CNS immune surveillance is an ongoing debate (Engelhardt et al., 2017), even though its unique character regarding the immune responses is undoubted (Louveau et al., 2015a). After understanding the cellular and molecular principles underlying the immune privileges of the CNS comprehensively, one can hope to find improved treatment options for neurological disorders such as multiple sclerosis (MS), Alzheimer's disease, and stroke (Engelhardt et al., 2017). One major player involved in the CNS immune responses are myelopoietic cells. Central myeloid cell populations in the CNS are parenchymal microglia and non-parenchymal macrophages, which can be sub-classified in perivascular macrophages, meningeal macrophages, macrophages of the choroid plexus, and blood-derived monocytes (Prinz et al., 2011). Non-parenchymal macrophages mediate immune responses at brain boundaries (Goldmann et al., 2016). The blood-derived monocytic cells can be recruited to the CNS under pathophysiological as well as inflammatory conditions and contribute to brain pathology (Mammana et al., 2018). They infiltrate mechanical lesion sites along with zones of acute, anterograde (Wallerian) axonal degeneration and transform into microglia-like cells (Bechmann et al., 2005). In addition, monocytes play a crucial role in the onset of MS, where they are associated with axonal loss, astrogliosis, and neurodegeneration (Kuhlmann et al., 2002; Slavin et al., 2010). In contrast, TREM2-transduced myeloid precursors limited tissue destruction and promoted CNS repair (Takahashi et al., 2007) in experimental autoimmune encephalomyelitis, the animal model for MS. Thus monocytes play a dual role and are also able to modulate postlesional plasticity and can serve as cellular carriers to transport therapeutic substances or small molecular agents into the CNS by bypassing the blood-brain barrier, protecting the CNS (Abbott et al., 2010). Monocytes, which are transporting agents through the blood-brain barrier into the CNS are also used in various other promising animal studies, for example in Parkinson's disease, where monocytes mediated transport of therapeutic nanozymes into the CNS plasma (Brynskikh et al., 2010). Another example of the importance of blood monocytes in diseases is their recruitment to the injured spinal cord where they promote recovery (Schwartz, 2010). Also, nanoparticle-loaded monocytes are attracted to epileptogenic brain tissue and could potentially be used for reducing the systemic dose of potentially toxic compounds (Han et al., 2019).

Since the first production of nanoparticles in the 1980s, their application potential concerning imaging and treatment of the CNS has increased significantly, for instance, in cancer therapy through magnetic hyperthermia or in vascular magnetic resonance imaging as contrast agents to visualize malformations. Especially superparamagnetic iron oxide nanoparticles (SPIO) were studied for a long time as contrast agents in magnetic resonance imaging (Rumenapp et al., 2012). Compared to conventional gadolinium-based contrast agents, they achieve a higher spatial resolution and therefore improve diagnostic accuracy (Shokrollahi, 2013). Many potential therapeutic applications for SPIO have been identified, including the treatment of brain tumors, MS, cerebral ischemia or stroke, carotid atherosclerosis, traumatic brain injury as well as epilepsy (Weinstein et al., 2010; Ittrich et al., 2013). As the first line of immune defense, the influence of SPIO on central myelopoietic cells such as macrophages, monocytes, and microglia is the highest. To evaluate the potential risks of applying nano-objects, their uptake, metabolization, and possible alterations affecting the functions or vitality of the myelopoietic cells have to be investigated thoroughly in animal studies before being applied in humans.

[1]Institute of Cell Biology and Neurobiology, Center for Anatomy, Charité- Universitätsmedizin Berlin, Berlin, Germany; [2]Department of Neurosurgery, Helios Klinikum Berlin Buch, Berlin, Germany
*Correspondence to: Jana Glumm, MD, jana.glumm@charite.de.
https://orcid.org/0000-0001-5756-3718 (Jana Glumm)

First attempts have been made to elucidate the effects of nanoparticles on blood-derived monocytes to predict their influence, once the CNS has been reached (Tong et al., 2016). However, the incubation of monocytes with nanoparticles could change their cellular integrity, differentiation rate, migratory ability, or physiological functions and might result in alterations of the targeted CNS environment (Neubert et al., 2015). Here, we describe the influence of carboxydextran-coated SPIO Resovist and citrate-coated VSOP (SPIO subgroup) on the vitality, cytokine, and chemokine secretion together with the iron uptake of murine blood-derived monocytes.

## Materials and Methods

### Animals
Adult C57BL/6 female mice (Charles River, Sulzbach, Germany) at the age of 6–8 weeks and the average body weight of 20 g were used for all experiments. Up to ten animals were kept in a cage with a constant 12-hour day/night rhythm, access to nest-building materials, a running wheel, and a supply of water and food *ad libitum*. Mice were bred and supplied by the Forschungseinrichtung für Experimentelle Medizin of the Charité-Universitätsmedizin Berlin, Germany. All experiments were carried out in conformity with the European guidelines (2010/63/EU) for the use of laboratory animals as well as the German Animal Welfare Act and were certified by the local regulatory authority of Berlin (Landesamt für Gesundheit und Soziales [LaGeSo]; registration number O_0097/11). All measures were taken to reduce the degree of suffering and the number of animals sacrificed to a minimum. In total, 104 mice were used for all experiments described below.

### Nanoparticles
VSOP were synthesized and supplied by the Charité Institute of Radiology (Taupitz et al., 2000). We used two citrate-coated VSOP composed of monocrystalline iron oxide cores of magnetite ($Fe_3O_4$) and maghemite ($\gamma$-$Fe_2O_3$), which have been characterized in detail before (Neubert et al., 2015; Pohland et al., 2017). Briefly summarized we applied two types of these nanoparticles: VSOP-R1 with a hydrodynamic diameter of 6.1 nm with 75% of particles within 4.1–7.5 nm and VSOP-R2 with a hydrodynamic diameter of 8.7 nm with 75% of particles within 6.5–10.1 nm.

VSOP-R1 were added in particle concentrations of 0.75 mM (41.87 mg iron/L). VSOP-R2 were applied in particle concentrations of 0.75 mM (41.9 mg iron/L). In addition, ultrasmall SPIO Resovist/Ferucarbotran (Bayer Pharma AG, Berlin, Germany) described by Reimer and Balzer (2003) were used at particle concentrations of 0.75 mM.

### Isolation and treatment of peripheral monocytes
Murine monocytes were isolated as described in detail previously (Kaminski et al., 2012). Briefly, mice were sedated, and peripheral blood was collected after puncturing the right atrium. Accordingly, blood was diluted, overlaid on a Histopaque 1083 sucrose solution (Sigma-Aldrich, St. Louis, MO, USA), and centrifuged at $400 \times g$ for 30 minutes at room temperature. Then, the mononuclear cell interface was washed and incubated in a suspension containing microbeads conjugated to rat anti-mouse cluster of differentiation molecule 11b (CD11b) monoclonal antibodies according to the supplier's instructions (Miltenyi Biotec, Bergisch Gladbach, Germany). After that CD11b-positive cell fraction was gained using a magnetic-activated cell separation kit (Miltenyi Biotec), whereas the negative fraction was discarded. Subsequently, the viability of CD11b-positive monocytes was quantified using a Neubauer chamber and Trypan Blue staining (Sigma-Aldrich). Cells were cultivated at a concentration of $1 \times 10^5$–$3 \times 10^5$/mL in Roswell Park Memorial Institute 1640 medium (Thermo Fisher Scientific, Waltham, MA, USA) containing 10% fetal calf serum (PAN-Biotech GmbH, Aidenbach, Germany) at 37°C in humidified 5% $CO_2$-enriched atmosphere for 1 day *in vitro* (DIV). VSOP-R1, -R2, and Resovist were added to the medium at a particle concentration of 0 mM (negative control) and 0.75 mM. Monocytic cytokine secretion was activated using *Escherichia coli* lipopolysaccharide (LPS) (Enzo Life Sciences, Inc., Farmingdale, NY, USA) at a concentration of 0.1 μg/mL. SPIO, as well as LPS stimulation, were performed for 24 hours. Supernatants were collected after 1, 3, 6, 12, and 24 hours of incubation for cytokine assay. Monocytic cell death was induced by 5 minutes of 4% paraformaldehyde (PFA) (Merck KGaA, Darmstadt, Germany) treatment.

### Immunohistochemistry, Prussian blue, and viability staining
Monocytes were cultivated for 1 DIV with and without SPIO treatment on poly-d-lysine (Sigma-Aldrich) coated glass slides. Then specimens were fixed with 4% PFA (Merck KGaA). Nuclear Fast Red (NFR) (Carl Roth, Karlsruhe, Germany) and Prussian blue staining procedures, embedding with Immu-Mount (Thermo Fisher Scientific) as well as coverslipping were performed as described before (Perl and Good, 1992; Tysiak et al., 2009).

For assessing morphologic characterizations, monocytes were stained after incubation with rat anti-mouse CD11b monoclonal antibody (mAb) overnight at 4°C (1:1000, RRID: AB_2829357; Leinco Technologies, St. Louis, MO, USA), goat anti-rat Alexa Fluor 568 mAb for 2 hours at room temperature (1:500, RRID: AB_2534121; Thermo Fisher Scientific), and 4',6-diamidino-2-phenylindole (DAPI) (Carl Roth) followed by embedding using Immu-Mount (Thermo Fisher Scientific) and coverslipping.

To analyze the total number as well as the amount of viable and dead cells, monocytes were stained using a cell viability imaging kit (Roche Diagnostics GmbH, Mannheim, Germany) in accordance with the manufacturer's

protocol. Briefly, 50 μL of dye mixture was added to 200 μL of the medium of each specimen followed by 30 minutes of incubation at 37°C in a humidified 5% $CO_2$-enriched atmosphere.

### Microscopy and live imaging
All immunofluorescence and bright-field images of fixed and stained monocytes were taken using an Olympus BX51 microscope equipped with narrow-band filters (Olympus, Tokyo, Japan) as well as a Magnafire digital camera and Magnafire 2.1B software (Intas, Göttingen, Germany). Adjustment of brightness, background, and contrast was accomplished via ImageJ version 1.52 (NIH, Bethesda, MD, USA) (Schneider et al., 2012).

After 24 hours of incubation with and without VSOP or SPIO treatment, long shots of unfixed monocytes were taken for live imaging by the use of an inverse Olympus IX81 microscope equipped with a motorized stage in a heated measuring chamber (37°C) with humidified $CO_2$-enriched atmosphere, an F-View II digital camera and Xcellence software (all from Olympus). Constant exposition and instrument settings were used for all measurements. In total, 15 specimens ($n = 3$) were analyzed which were obtained from one experimental setup using $2 \times 10^5$ cells per well (three samples for untreated negative control, three samples for 0.75 mM VSOP-R1, three samples for 0.75 mM VSOP-R2, three samples for 0.75 mM Resovist, and three samples for 4% PFA). For this, three images of individual sectors were taken in each well for every staining. Data collection, as well as background, brightness, and contrast modifications, were performed using ImageJ. The amount of vital (calcein acetoxymethyl ester (Calcein-AM)-positive) and dead (propidium iodide (PI)-positive) monocytes was calculated as a ratio in % compared to the total counted cell number (Hoechst 33342-positive). In total, 34 mice were used for microscopical analysis.

### Lactate dehydrogenase activity
For assessing monocytes' integrity, determination of lactate dehydrogenase (LDH) activity in cell culture supernatants was performed using a Cytotoxicity Assay Kit (Cayman Chemical Company, Ann Arbor, MI, USA) in accordance with the manufacturer's protocol.

### Cytokine and chemokine evaluation
The quantity of C-X-C motif chemokine (CXCL1)/KC, granulocyte-macrophage colony-stimulating factor (GM-CSF), interleukin (IL)-6, interferon-gamma induced protein; 10 kDa (IP-10), monocyte chemoattractant protein (MCP)-1 plus -3, macrophage inflammatory protein-1 alpha, and beta (MIP-1α/β) as well as tumor necrosis factor (TNF)-α in monocyte cell culture supernatants was verified with a bead-based multiple analyte immunoassay (FlowCytomix) in accordance with the manufacturer's manual (eBioscience, San Diego, CA, USA). Measurements were performed using double determinations of every specimen. Analysis and data evaluation were carried out by the use of a FACSCanto II flow cytometer equipped with FACSDiva software (both from BD Bioscience, Franklin Lakes, NJ, USA) and Flowcytomix software (eBioscience). In total, 50 supernatants were analyzed (10 samples for untreated negative control, 10 samples for 0.1 μg/mL LPS, 10 samples for 0.75 mM VSOP-R1, 10 samples for 0.75mM VSOP-R2, 10 samples for 0.75 mM Resovist) which were obtained from two different experimental setups using $1 \times 10^5$ and $3 \times 10^5$ cells per specimen respectively. In total, 70 mice were used for cytokine and chemokine analysis as well as magnetic particle spectroscopy (MPS) iron quantification.

### MPS for iron quantification
After 1, 3, 6, 12, and 24 hours of incubation with or without 0.75 mM VSOP-R1, 0.75 mM VSOP-R2, and 0.75 mM Resovist, monocytes specimens ($1 \times 10^5$ cells in each treatment group) were washed with 0.1 M PBS. Subsequently, cell pellets were transferred into a polymerase chain reaction tube. MPS was performed as described previously (Pohland et al., 2017). In total, 40 samples were analyzed from one experimental setup (two individual samples for every treatment and each time point). Untreated samples incubated without VSOP or SPIO served as negative control (data not shown). Data illustration was performed with GraphPad Prism 9.2.0 (GraphPad Software, San Diego, CA, USA; www.graphpad.com).

### Ultraviolet-visible spectroscopy
VSOP-R1, VSOP-R2, and Resovist were diluted in distilled water at a particle concentration of 3mM. Absorption was measured in a wavelength range from 420 nm to 600 nm using a Cary 100 Scan photometer equipped with Cary WinUV software (both from Agilent Technologies, Mulgrave, Australia) and 10 mm quartz cuvettes (Hellma, Muellheim, Germany).

### Statistical analysis
Data are presented as mean ± standard deviation (SD). All statistical analyses were performed with GraphPad Prism software. Statistical analysis of live imaging and LDH measurement were conducted using one-way analysis of variance and Tukey's *post hoc* test. Statistical analysis of cytokine and chemokine measurement was performed using two-way analysis of variance and Tukey's *post hoc* test. $P < 0.05$ was considered statistically significant.

## Results

### The vitality of untreated monocytes after incubation
After 1DIV, monocytes were visualized by immunofluorescence staining to verify an intact cellular structure. Using CD11b and DAPI labeling (**Additional Figure 1**), we were able to prove maintained monocytic characteristics (e.g. kidney-shaped nucleus) in course of the experimental setup (**Figure 1A**). In

addition, a viability assay was performed after 1 DIV to analyze the amount of dying or dead monocytes that have lost their membrane integrity. Exemplary images of untreated monocytes stained with Hoechst 33342, PI, and Calcein-AM are shown in **Figure 1B** first row. We quantified the negative control and found an average percentage of ~77.9% vital monocytes (**Figure 1C**).

### Decrease of monocyte viability is treatment-dependent

The influence of VSOP-R1,-R2, and Resovist on murine monocytes' vitality was tested over a 1DIV incubation period at a concentration of 0.75 mM each. Representative images of VSOP-R1 treated cells are shown in **Figure 1B** row 2, for VSOP-R2 in **Figure 1B** row 3 as well as for Resovist in **Figure 1B** row 4. Cell death was induced using 4% PFA treatment which served as the positive control (**Figure 1B** last row 5). While the total cell number (Hoechst 33342 staining) is more or less constant in all specimens depicted (**Figure 1B**), an SPIO, as well as PFA-dependent decrease of Calcein-AM-positive (vital) and increase of PI-positive (dying or dead) monocytes, is visible, compared to the negative untreated control. These results are in line with the statistical analysis, representing the calculated ratio in % of vital (**Figure 1C**) and dead monocytes in proportion to the total cell number (**Figure 1D**). Here, we observed a significant vitality loss of ~28.9% for VSOP-R1 incubated samples. In contrast, VSOP-R2 treatment intensified cell death and resulted in a viability reduction of ~54.8%, whereas Resovist application decreased monocytic integrity by ~35.0%. In comparison, PFA incubation maximized cell death and reduced the average cell vitality substantially to a minimum of ~7.7%.

We have measured the LDH activity for VSOP-R1, VSOP-R2, Resovist, and control (**Figure 1E**). Only in the VSOP-R2 treatment group was a statistically significant increase in LDH activity detected ($P < 0.05$) compared to the untreated control.

### Monocytes accumulate VSOP and Resovist

After 1 DIV, monocytes were labeled to verify their VSOP and Resovist uptake (**Figure 2B–D**). For this purpose, cells were incubated with and without 0.75 mM VSOP-R1, -R2, and Resovist. Subsequently, we used NFR and PB iron staining to visualize the cellular structure and iron deposits respectively and demonstrated the non-existence of iron around or within cell bodies of the untreated control (**Figure 2A**). In contrast, we confirmed the presence of iron in monocytic specimens treated with VSOP-R1 (**Figure 2B**), VSOP-R2 (**Figure 2C**), and Resovist (**Figure 2D**).

### VSOP treatment does not alter monocytic cytokine secretion

During nanoparticle treatment, we determined the monocytic cytokine homeostasis with regards to stimulating, as well as, pro- and anti-inflammatory molecules in specimen supernatants. From 1 to 24 hours of incubation, we were able to verify the release of CXCL/KC, IL-6, IP-10, MIP-1α, MIP-1β, and TNF-α utilizing our experimental setup (**Figure 2E–J**). The statistical evaluation proved no changes in VSOP-R1, VSOP-R2, or Resovist-treated samples compared with the negative control. Compared to all treatment groups and time points, a significant effect ($P < 0.01$) was exclusively detectable for MIP-1α secretion after 24 hours of incubation in the LPS-stimulated samples (**Figure 2H**). In addition, neither LPS nor nanoparticle incubation activated a GM-CSF, MCP-1, and MCP-3 release (data not depicted). Also, a relatively high SD for all measuring points has to be noted.

### VSOP uptake seem to be nanoparticle- and time-dependent

Nanoparticle uptake was analyzed between 1 hour and 24 hours of incubation via MPS. The quantified iron content of the untreated negative control served as zero value and was subtracted from each measurement shown in **Figure 2K**. We attributed the general iron basis level to the magnetic microbead-conjugated antibodies applied in terms of cell separation. MPS analysis confirmed the uptake of VSOP-R1,-R2, and Resovist. We found the highest uptake in VSOP-R1 treated samples with a constant increase during incubation. In contrast, VSOP-R2 absorption stagnated after 6 hours and was approximately reduced by 40–50% compared to VSOP-R1. Resovist uptake was detectable at all time points measured. However, compared to VSOP-R1 and VSOP-R2, it remained at a consistently low level. We excluded statistical analysis due to the small amount of data required and have added this information as a proof of principle.

### Ultraviolet-visible spectroscopy shows differences in the SPIO absorption properties

We identified three divergent absorption spectra that decreased with increasing wavelength and gradually converged (**Additional Figure 1B**). While VSOP-R1 and VSOP-R2 showed only minor differences, a significantly higher absorption was detectable for Resovist.

## Discussion

Nanoparticles have become an integral part of our everyday life, for example, in agriculture, cosmetics, and food production, material engineering or in the pharmaceutical industry. Due to their small size, they facilitate an increased chemical reactivity and bioavailability that correlates with their high surface-to-volume ratio (Kessler, 2011; Contado, 2015). However, the benefits and risks of applying nanoparticles which probably penetrate various organs, tissues, and cells during their systemic circulation have to be considered carefully. The safety of nanoparticles penetrating the CNS has to be ensured. For this reason, detailed information about the nanoparticle-dependent release, translocation, elimination, metabolism, induced toxicity, or labeling-efficacy using blood-derived monocytes are mandatory and should be collected for further conclusions.
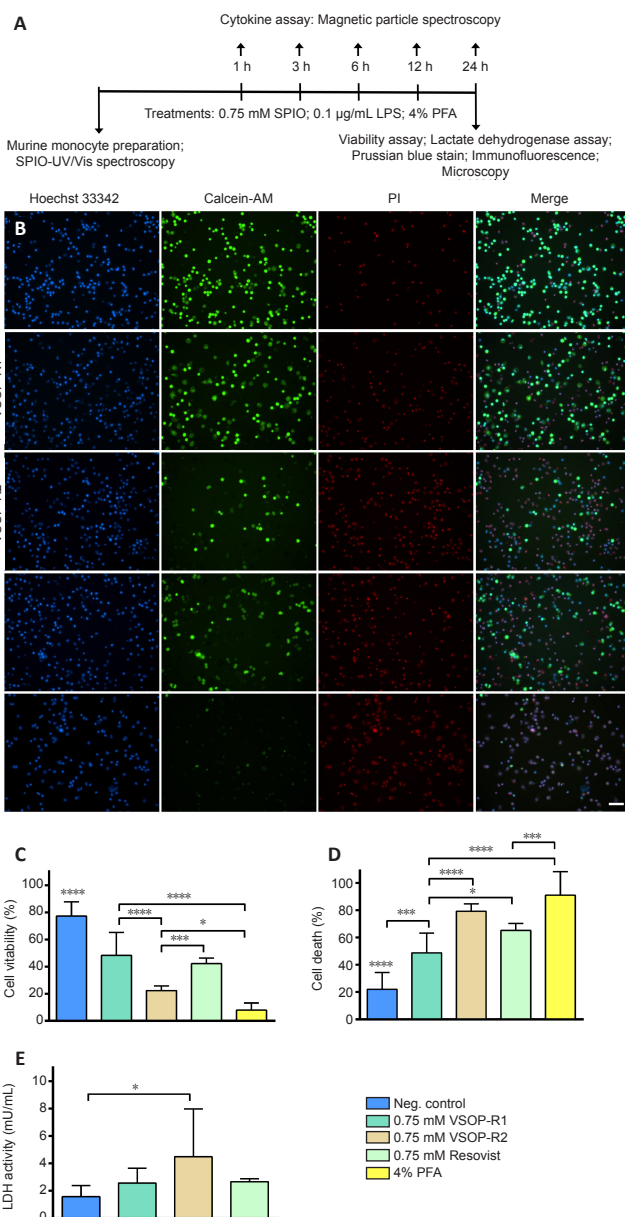


**Figure 1 | Superparamagnetic iron oxide nanoparticles (SPIO) exposure affects monocyte viability.**

(A) Experimental setup. (B) Fluorescence live-images of representative nuclear-stained monocytes taken after 1 DIV of treatment with and without different SPIO as well as 4% of paraformaldehyde (PFA). Scale bar: 50 μm. The first row represents monocytes incubated without any treatment, the second row shows monocytes incubated with 0.75 mM VSOP-R1 (hydrodynamic diameter of 6.1 nm with 75% of particles within 4.1–7.5 nm), the third row depicts monocytes incubated with 0.75 mM VSOP-R2 (hydrodynamic diameter of 8.7 nm with 75% of particles within 6.5–10.1 nm), the fourth row represents monocytes incubated with 0.75 mM Resovist (SPIO), the last row shows monocytes incubated with 4% PFA. Ubiquitous Hoechst 33342 nuclear staining (blue) defines all monocytes, Calcein-AM nuclei labeling (green) visualizes vital monocytes, fluorescent intercalating agent PI (red) stains apoptotic and dead monocytes. The last column shows merges of pictures shown for each treatment group. (C and D) Normalized monocyte viability (C) and cell death (D) measured after 1DIV of treatment with and without different SPIO as well as 4% PFA show a nanoparticle-dependent decrease in viability (one-way analysis of variance and Tukey's *post hoc* test: error bars represent SD, number of triple determinations for all groups: $n = 3$; *$P < 0.05$, ***$P < 0.001$, ****$P < 0.0001$). (E) Lactate dehydrogenase assay measured after 1DIV of treatment with and without different SPIO indicate for a VSOP-R2-dependent loss of cell integrity (one-way analysis of variance and Tukey's *post hoc* test; error bars represent SD, number of triple determinations for all groups: $n = 3$; *$P < 0.05$). DIV: day *in vitro*; LDH: lactate dehydrogenase; LPS: lipopolysaccharide; Neg.: negative; PFA: paraformaldehyde; PI: propidium iodide; SD: standard deviation; SPIO: superparamagnetic iron oxide nanoparticles; UV/Vis: ultraviolet-visible; VSOP: very small superparamagnetic iron oxide particles.

As recently discovered, the Food and Drug Administration approved carbohydrate-coated SPIO Ferumoxytol (indicated for the treatment of iron deficiency anemia) can cause fatal, adverse reactions including serious hypersensitivity and anaphylaxis after intravenous injection (Alsaleh and Brown, 2020).
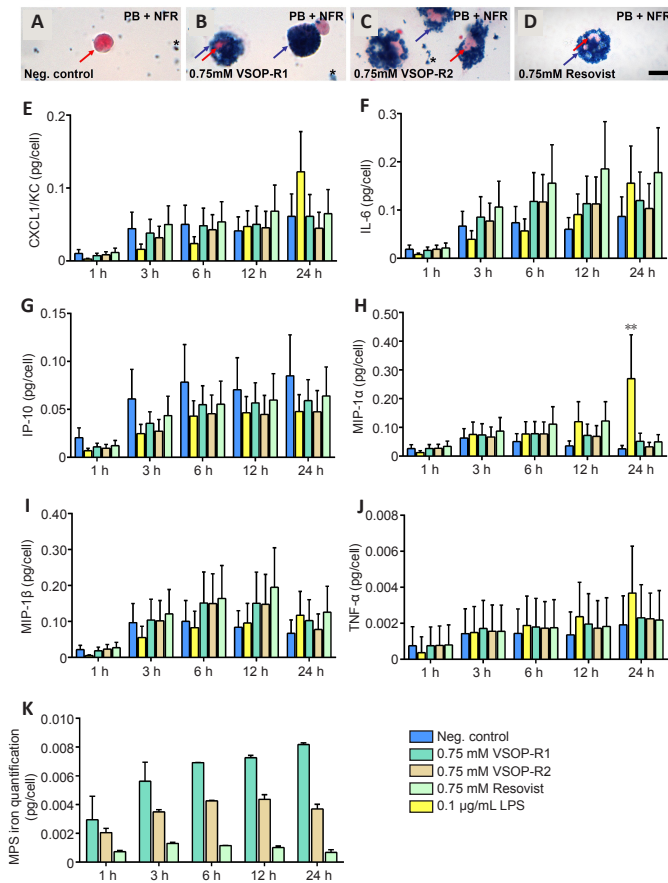
**Figure 2 | Nanoparticle uptake does not affect cytokine secretion of monocytes.**
(A–D) Bright-field images of peripheral monocytes after 1DIV of treatment with and without different VSOP as well as Prussian blue (PB) and Nuclear Fast Red (NFR) staining. Scale bar: 10 µm. (A) Monocyte incubated without any treatment shows characteristic kidney-shaped nucleus (red arrow) and PB-positive artifacts (black asterisk). (B) Monocytes treated with 0.75 mM VSOP-R1 (hydrodynamic diameter of 6.1 nm with 75% of particles within 4.1–7.5 nm) were almost covered with PB-positive iron particles (blue arrows). (C) Monocytes incubated with 0.75 mM VSOP-R2 (hydrodynamic diameter of 8.7 nm with 75% of particles within 6.5–10.1 nm). (D) Monocytes incubated with 0.75mM Resovist (SPIO). (E–K) Monocytic cytokine secretion measured between 1 hour and 24 hours of treatment with and without different SPIO indicates no nanoparticle-induced effects (two-way analysis of variance and Tukey's *post hoc* test: error bars represent standard deviation (SD); the number of double determinations for all graphs: $n = 2$; **$P < 0.01$). (E) CXCL/KC. (F) IL-6. (G) IP-10. (H) MIP-1α. (I) MIP-1β. (J) TNF-α. (K) MPS iron quantification after 1–24 hours of SPIO treatment (error bars represent SD; the number of double determinations: $n = 1$). CXCL1/KC: c-x-c-motif ligand 1; DIV: day *in vitro*; IL: interleukin; IP: interferon gamma-induced protein; LPS: lipopolysaccharide; MIP: macrophage inflammatory protein; MPS: magnetic particle spectroscopy; Neg.: negative; NFR: Nuclear Fast Red; PB: Prussian Blue; SD: standard deviation; SPIO: superparamagnetic iron oxide nanoparticles; TNF: tumor necrosis factor; VSOP: very small superparamagnetic iron oxide particles.

In this study, we analyzed the influence of Resovist, VSOP-R1, and -R2 on the viability, cytokine, and chemokine homeostasis as well as the iron uptake of murine blood-derived monocytes. We have already been able to prove that the separation method implemented ensures a monocytes purification > 91% (CD11b-positive/CD11c-negative) and a viability > 94% together with a yield of $5 \times 10^4$–$15 \times 10^4$ cells per processed milliliter of blood (Kaminski et al., 2012). Consequently, we have not presented these results again in this approach. We applied immunofluorescence and histochemical stainings to confirm intact monocytic cell integrity and cytoarchitecture (e.g. ubiquitous CD11b expression, kidney-shaped nucleus, and nucleus-to-cytoplasm ratio; **Additional Figure 1A**) in the course of our experimental setup. Publications evaluating the impact of SPIO are limited and particle dose and exposure time are still discussed controversially (Stroh et al., 2005; Lu et al., 2007; Foldager et al., 2011; Sun et al., 2014). However, we have described VSOP concentrations of 0.5 to 3.0 mM in our view as clinically relevant, as they mimic the peak effect range after bolus dosing *in vivo* (Neubert et al., 2015; Pohland et al., 2017). Here, we used an incubation time of up to 1DIV and a specific nanoparticle concentration of 0.75mM in all treatment groups. These conditions are in correspondence with previously published data for the human acute monocytic leukemia cell line THP-1 (Ludwig et al., 2013).

Our first set of experiments was conducted to evaluate whether the contrast agents applied affect the survival of monocytes during a 24-hour exposure. As described, cell death of ~17% (in contrast to vitality after enrichment, data not shown) was detected in the negative control. We assume that the moderate decline was generally caused by blood processing associated stress affecting all treatment groups. Compared to the reference (untreated

monocytes), VSOP-R1-incubated samples showed a significant loss of their cellular integrity (~29%). The VSOP-R2 treatment intensified mortality by overall ~55%, whereas Resovist reduced monocytes' vitality by ~35.0%. The PFA-fixed positive control boosted cell death and minimized the average cell viability markedly to ~7.7%.

Although LDH measurement can be influenced by the presence of SPIO, we found in our study that incubation of monocytes with VSOP-R2 leads to increased cell death. This is also reflected in the viability assay.

Since our results suggest that VSOP-R2 changed the cell integrity of the monocytes the most (although Resovist shows a significantly stronger self-absorption), we assume that this could indeed be the influence of the nanoparticles used. In addition, this result also reflects the tendency from the viability assay. Because SPIOs can affect measurements due to their characteristics, methods must be chosen that are less susceptible to interferences.

VSOP-R1 and -R2 are electrostatically stabilized by a citrate coating, bear a negative surface charge, and differ slightly for instance, in their hydrodynamic diameter and Z-average measured by dynamic light scattering (Taupitz et al., 2000; Wagner et al., 2002). In comparison, Resovist has a hydrodynamic diameter of ~60 nm, a composition of 0.5 mol Fe/L, 40 mg/mL mannitol as well as 2 mg/mL lactic acid, and is according to its carboxydextran-coating also negatively charged (Reimer and Balzer, 2003). Even though all nanoparticles applied reduced monocytes' vitality significantly, differences between the treatment groups are obvious. Since all agents were utilized with equal total iron content and exposure time, we believe that the cell survival depended on the size, surface, and/or composition of the nanoparticles used. Interestingly, Neubert et al. (2015) found no differences between VSOP-R1 and VSOP-R2 in comparison to the larger-sized nanoparticle Resovist for example for the rapid accumulation by microglial cells. Whereas in our study, VSOP-R1 and VSOP-R2 were taken up much faster. Further studies are needed for consistent findings, allowing interpretation of this data.

In addition, primary murine monocytes appear more sensitive to SPIO exposure compared to the equivalent human cell line. Using similar incubation parameters VSOP and Resovist showed no effects on THP-1 derived monocytes (Ludwig et al., 2013). On the other hand, our results are comparable with a previously publicized report analyzing the viability of primary microglia during 6 hours of SPIO short-term exposure in concentrations of 0.5–1.5 mM (Neubert et al., 2015). We, therefore, conclude that the impact of the nanoparticles closely depends on the plasticity of the target cells used.

As described, we have demonstrated an accumulation of VSOP-R1, -R2, and Resovist. Based on the images received, we suspect both extracellular and intracellular iron deposits for all treatment groups exist. To clarify nanoparticle attachment or uptake in detail, further investigations using ultrathin sections electron micrographs (facilitating higher magnification and resolution) would be beneficial. Using electron microscopy, Resovist was detected especially in THP-1 intracellular vesicles. In contrast, VSOP were confirmed in aggregates on the cell surface, in vesicles and in distributed internal structures. Additionally, VSOP showed a high extracellular binding affinity for glycosaminoglycans plus apoptotic debris and membrane vesicles (Ludwig et al., 2013). Interestingly, recently published data prove a VSOP binding to the THP-1 glycocalyx that occurs within seconds after being applied to a cell suspension (Poller et al., 2020).

Monocytes circulate in the body to recognize foreign structures to destroy them by phagocytosis and initiation of the acquired immune response. This is induced by antigen presentation and the release of activating molecules like cytokines. For this reason, analysis of their secretion allows conclusions to be drawn about the biocompatibility of a substance. Cytokines, including chemokines (such as CXCL1/KC, GM-CSF, IP-10, MIP-1α, MIP-1β, MCP-1, MCP-3 IL-6, and TNF-α) which we have focused on in this study, are small proteins that mediate signaling and cell interaction during inflammatory processes. Among other things, they are not only responsible for leukocytes recruitment, positioning, accumulation as well as induction of phagocytosis and production of reactive oxygen species but also for cell differentiation and survival (Miyagishi et al., 1997; Baggiolini, 1998; Laurenzi et al., 2001; Streit et al., 2001; Ramesh et al., 2013; De Feo et al., 2017). Pathological overexpression of cytokine is linked with severe degenerative diseases including MS, Parkinson's disease, AD as well as human immunodeficiency virus-associated dementia (Ramesh et al., 2013). Nonetheless, there is evidence that cytokines can also have a healing effect (Kremlev et al., 2004).

As shown in our secretion assay, we found a time- but not a treatment-dependent increase of cytokine production, confirming a monocytic immune competence. Nanoparticles had therefore no impact and their results were comparable to the negative control, although VSOP-R1, -R2, and Resovist significantly elevated cell death. Admittedly, values of LPS endotoxin-stimulated specimens remained below our expectations, since we had assumed a substantial upregulation in advance. However, our results are comparable to former publications demonstrating that iron oxide nanoparticles do not necessarily affect cytokine homeostasis when applied to monocytes, microglia, or OHSC (Wang et al., 2011; Ludwig et al., 2013; Pohland et al., 2017).

In our last experiment, we characterized the uptake of VSOP-R1, -R2, and Resovist using MPS. MPS is a quick, sensitive, and cell-preserving

quantification method which can provide information about the content, binding characteristic, internalization, and biodegradation of a substance based on its magnetic properties (Ludwig et al., 2013; Poller et al., 2016, 2018, 2020). For this reason, MPS analysis offers diverse advantages when compared with destructive techniques such as colorimetric phenanthroline measurement (Ludwig et al., 2013).

As shown, the uptake seemed to be nanoparticle- and time-dependent and overall consistent with the results gained by (Ludwig et al., 2013). The iron content of VSOP-R1 treated samples constantly increased during incubation and was the highest altogether. In contrast, VSOP-R2 accumulation stagnated after 6h and possibly reached a saturation level. Furthermore, Resovist was detectable but its quantity was more or less consistently low, potentially indicating a reduced monocytic attraction or responsiveness. We, therefore, believe that a 6-hour treatment with 0.75 mM VSOP-R1 is probably sufficient to effectively label monocytes for future experiments. Our data also partly corresponds with study outcomes analyzing the effects of VSOP and Resovist on THP-1. The latest findings are, in our point of view, encouraging and expanding the knowledge of magnetically labeling monocytes for *in vivo* applications prospectively.

We are conscious that all results show a relatively high standard deviation that is related to the reduced number of tests. Additionally, the data presented is inadequate to fully understand the nanoparticle uptake mechanisms of murine blood-derived monocytes in detail. In our opinion, however, we have taken important steps to gain deeper insights into the magnetic labeling of primary immune cells.

Working with murine monocytes is challenging as their count in whole blood is minimal and their processing yield is correspondingly low due to the complexity in enrichment. It is essential nevertheless, as their metabolism and vitality differ immensely from equivalent tumor cell lines. One might argue that human monocytes can be easily isolated in large quantities from a buffy coat via surface marker CD14. However, if magnetic labeling is aimed at magnetic resonance imaging tracking of migrating living cells *in vivo*, then animal testing trials using mice or similar organisms and application of species-specific cells is the only safe option.

Optimized isolation and labeling strategy are mandatory, further experiments are required to clarify questions regarding nanoparticle accumulation, phagocytosis or their degradation. Subsequent tests should achieve a higher statistical significance. We are convinced that the results shown here are a small contribution to the characterization of SPIO for future trials. Based on our findings, we will continue to work with VSOP-R1 instead of VSOP-R2 or Resovist in a concentration of 0.75mM or less and try to reduce the incubation time to the minimum.

**Author contributions:** *MP designed the study, performed the experiments, collected data, evaluated results and drafted the manuscript. CP provided technical assistance, collected data and revised the manuscript. JK designed the study and revised the manuscript. JG supervised experiments, drafted and revised the manuscript. All authors approved the final version of this manuscript.*
**Conflicts of interest:** *The authors report no conflicts of interest in this work. MP and CP are siblings.*
**Availability of data and materials:** *All data generated or analyzed during this study are included in this published article and its supplementary information files.*
**Open peer reviewer:** *Qing You, Otto-von-Guericke University Magdeburg, Germany.*
**Additional file:**
*Additional Figure 1: Monocyte morphology and SPIO absorption.*

# References

Abbott NJ, Patabendige AA, Dolman DE, Yusof SR, Begley DJ (2010) Structure and function of the blood-brain barrier. Neurobiol Dis 37:13-25.
Alsaleh NB, Brown JM (2020) Engineered nanomaterials and type I allergic hypersensitivity reactions. Front Immunol 11:222.
Baggiolini M (1998) Chemokines and leukocyte traffic. Nature 392:565-568.
Bechmann I, Goldmann J, Kovac AD, Kwidzinski E, Simburger E, Naftolin F, Dirnagl U, Nitsch R, Priller J (2005) Circulating monocytic cells infiltrate layers of anterograde axonal degeneration where they transform into microglia. FASEB J 19:647-649.
Billingham RE, Boswell T (1953) Studies on the problem of corneal homografts. Proc R Soc Lond B Biol Sci 141:392-406.
Brynskikh AM, Zhao Y, Mosley RL, Li S, Boska MD, Klyachko NL, Kabanov AV, Gendelman HE, Batrakova EV (2010) Macrophage delivery of therapeutic nanozymes in a murine model of Parkinson's disease. Nanomedicine (Lond) 5:379-396.
Contado C (2015) Nanomaterials in consumer products: a challenging analytical problem. Front Chem 3:48.
De Feo D, Merlini A, Brambilla E, Ottoboni L, Laterza C, Menon R, Srinivasan S, Farina C, Garcia Manteiga JM, Butti E, Bacigaluppi M, Comi G, Greter M, Martino G (2017) Neural precursor cell-secreted TGF-beta2 redirects inflammatory monocyte-derived cells in CNS autoimmunity. J Clin Invest 127:3937-3953.

Engelhardt B, Vajkoczy P, Weller RO (2017) The movers and shapers in immune privilege of the CNS. Nat Immunol 18:123-131.
Foldager CB, Pedersen M, Ringgaard S, Bunger C, Lind M (2011) Chondrocyte gene expression is affected by very small iron oxide particles-labeling in long-term in vitro MRI tracking. J Magn Reson Imaging 33:724-730.
Goldmann T, Wieghofer P, Jordão MJ, Prutek F, Hagemeyer N, Frenzel K, Amann L, Staszewski O, Kierdorf K, Krueger M, Locatelli G, Hochgerner H, Zeiser R, Epelman S, Geissmann F, Priller J, Rossi FM, Bechmann I, Kerschensteiner M, Linnarsson S, et al. (2016) Origin, fate and dynamics of macrophages at central nervous system interfaces. Nat Immunol 17:797-805.
Han H, Eyal S, Portnoy E, Mann A, Shmuel M, Benifla M, Ekstein D, Polyak B (2019) Monocytes as Carriers of Magnetic Nanoparticles for Tracking Inflammation in the Epileptic Rat Brain. Curr Drug Deliv 16:637-644.
Ittrich H, Peldschus K, Raabe N, Kaul M, Adam G (2013) Superparamagnetic iron oxide nanoparticles in biomedicine: applications and developments in diagnostics and therapy. Rofo 185:1149-1166.
Kaminski M, Bechmann I, Pohland M, Kiwit J, Nitsch R, Glumm J (2012) Migration of monocytes after intracerebral injection at entorhinal cortex lesion site. J Leukoc Biol 92:31-39.
Kessler R (2011) Engineered nanoparticles in consumer products: understanding a new ingredient. Environ Health Perspect 119:a120-125.
Kremlev SG, Roberts RL, Palmer C (2004) Differential expression of chemokines and chemokine receptors during microglial activation and inhibition. J Neuroimmunol 149:1-9.
Kuhlmann T, Lingfeld G, Bitsch A, Schuchardt J, Bruck W (2002) Acute axonal damage in multiple sclerosis is most extensive in early disease stages and decreases over time. Brain 125:2202-2212.
Laurenzi MA, Arcuri C, Rossi R, Marconi P, Bocchini V (2001) Effects of microenvironment on morphology and function of the microglial cell line BV-2. Neurochem Res 26:1209-1216.
Louveau A, Harris TH, Kipnis J (2015a) Revisiting the Mechanisms of CNS Immune Privilege. Trends Immunol 36:569-577.
Louveau A, Smirnov I, Keyes TJ, Eccles JD, Rouhani SJ, Peske JD, Derecki NC, Castle D, Mandell JW, Lee KS, Harris TH, Kipnis J (2015b) Structural and functional features of central nervous system lymphatic vessels. Nature 523:337-341.
Lu CW, Hung Y, Hsiao JK, Yao M, Chung TH, Lin YS, Wu SH, Hsu SC, Liu HM, Mou CY, Yang CS, Huang DM, Chen YC (2007) Bifunctional magnetic silica nanoparticles for highly efficient human stem cell labeling. Nano Lett 7:149-154.
Ludwig A, Poller WC, Westphal K, Minkwitz S, Lattig-Tunnemann G, Metzkow S, Stangl K, Baumann G, Taupitz M, Wagner S, Schnorr J, Stangl V (2013) Rapid binding of electrostatically stabilized iron oxide nanoparticles to THP-1 monocytic cells via interaction with glycosaminoglycans. Basic Res Cardiol 108:328.
Mammana S, Fagone P, Cavalli E, Basile MS, Petralia MC, Nicoletti F, Bramanti P, Mazzon E (2018) The role of macrophages in neuroinflammatory and neurodegenerative pathways of Alzheimer's disease, amyotrophic lateral sclerosis, and multiple sclerosis: pathogenetic cellular effectors and potential therapeutic targets. Int J Mol Sci 19.
Miyagishi R, Kikuchi S, Takayama C, Inoue Y, Tashiro K (1997) Identification of cell types producing RANTES, MIP-1 alpha and MIP-1 beta in rat experimental autoimmune encephalomyelitis by in situ hybridization. J Neuroimmunol 77:17-26.
Neubert J, Wagner S, Kiwit J, Brauer AU, Glumm J (2015) New findings about iron oxide nanoparticles and their different effects on murine brain primary cells. Int J Nanomedicine 10:2033-2049.
Perl DP, Good PF (1992) Comparative techniques for determining cellular iron distribution in brain tissues. Ann Neurol 32 Suppl:S76-81.
Pohland M, Glumm R, Wiekhorst F, Kiwit J, Glumm J (2017) Biocompatibility of very small superparamagnetic iron oxide nanoparticles in murine organotypic hippocampal slice cultures and the role of microglia. Int J Nanomedicine 12:1577-1591.
Poller WC, Lowa N, Schleicher M, Munster-Wandowski A, Taupitz M, Stangl V, Ludwig A, Wiekhorst F (2020) Initial interaction of citrate-coated iron oxide nanoparticles with the glycocalyx of THP-1 monocytes assessed by real-time magnetic particle spectroscopy and electron microscopy. Sci Rep 10:3591.
Poller WC, Lowa N, Wiekhorst F, Taupitz M, Wagner S, Moller K, Baumann G, Stangl V, Trahms L, Ludwig A (2016) Magnetic particle spectroscopy reveals dynamic changes in the magnetic behavior of very small superparamagnetic iron oxide nanoparticles during cellular uptake and enables determination of cell-labeling efficacy. J Biomed Nanotechnol 12:337-346.
Poller WC, Pieber M, Boehm-Sturm P, Ramberger E, Karampelas V, Moller K, Schleicher M, Wiekhorst F, Lowa N, Wagner S, Schnorr J, Taupitz M, Stangl K, Stangl V, Ludwig A (2018) Very small superparamagnetic iron oxide nanoparticles: Long-term fate and metabolic processing in atherosclerotic mice. Nanomedicine 14:2575-2586.
Prinz M, Priller J, Sisodia SS, Ransohoff RM (2011) Heterogeneity of CNS myeloid cells and their roles in neurodegeneration. Nat Neurosci 14:1227-1235.
Ramesh G, MacLean AG, Philipp MT (2013) Cytokines and chemokines at the crossroads of neuroinflammation, neurodegeneration, and neuropathic pain. Mediators of inflammation 2013:480739.
Reimer P, Balzer T (2003) Ferucarbotran (Resovist): a new clinically approved RES-specific contrast agent for contrast-enhanced MRI of the liver: properties, clinical development, and applications. Eur Radiol 13:1266-1276.
Rumenapp C, Gleich B, Haase A (2012) Magnetic nanoparticles in magnetic resonance imaging and diagnostics. Pharm Res 29:1165-1179.
Schwartz M (2010) "Tissue-repairing" blood-derived macrophages are essential for healing of the injured spinal cord: from skin-activated macrophages to infiltrating blood-derived cells? Brain Behav Immun 24:1054-1057.
Shokrollahi H (2013) Contrast agents for MRI. Mater Sci Eng C Mater Biol Appl 33:4485-4497.
Slavin A, Kelly-Modis L, Labadia M, Ryan K, Brown ML (2010) Pathogenic mechanisms and experimental models of multiple sclerosis. Autoimmunity 43:504-513.
Streit WJ, Conde JR, Harrison JK (2001) Chemokines and Alzheimer's disease. Neurobiol Aging 22:909-913.
Stroh A, Faber C, Neuberger T, Lorenz P, Sieland K, Jakob PM, Webb A, Pilgrimm H, Schober R, Pohl EE, Zimmer C (2005) In vivo detection limits of magnetically labeled embryonic stem cells in the rat brain using high-field (17.6 T) magnetic resonance imaging. Neuroimage 24:635-645.
Sun Z, Worden M, Wroczynskyj Y, Yathindranath V, van Lierop J, Hegmann T, Miller DW (2014) Magnetic field enhanced convective diffusion of iron oxide nanoparticles in an osmotically disrupted cell culture model of the blood-brain barrier. Int J Nanomedicine 9:3013-3026.
Takahashi K, Prinz M, Stagi M, Chechneva O, Neumann H (2007) TREM2-transduced myeloid precursors mediate nervous tissue debris clearance and facilitate recovery in an animal model of multiple sclerosis. PLoS Med 4:e124.
Taupitz M, Schnorr J, Abramjuk C, Wagner S, Pilgrimm H, Hunigen H, Hamm B (2000) New generation of monomer-stabilized very small superparamagnetic iron oxide particles (VSOP) as contrast medium for MR angiography: preclinical results in rats and rabbits. J Magn Reson Imaging 12:905-911.
Tong HI, Kang W, Shi Y, Zhou G, Lu Y (2016) Physiological function and inflamed-brain migration of mouse monocyte-derived macrophages following cellular uptake of superparamagnetic iron oxide nanoparticles-Implication of macrophage-based drug delivery into the central nervous system. Int J Pharm 505:271-282.
Tysiak E, Asbach P, Aktas O, Waiczies H, Smyth M, Schnorr J, Taupitz M, Wuerfel J (2009) Beyond blood brain barrier breakdown- in vivo detection of occult neuroinflammatory foci by magnetic nanoparticles in high field MRI. J Neuroinflammation 6:20.
Wagner S, Schnorr J, Pilgrimm H, Hamm B, Taupitz M (2002) Monomer-coated very small superparamagnetic iron oxide particles as contrast medium for magnetic resonance imaging: preclinical in vivo characterization. Invest Radiol 37:167-177.
Wang Y, Wang B, Zhu MT, Li M, Wang HJ, Wang M, Ouyang H, Chai ZF, Feng WY, Zhao YL (2011) Microglial activation, recruitment and phagocytosis as linked phenomena in ferric oxide nanoparticle exposure. Toxicol Lett 205:26-37.
Weinstein JS, Varallyay CG, Dosa E, Gahramanov S, Hamilton B, Rooney WD, Muldoon LL, Neuwelt EA (2010) Superparamagnetic iron oxide nanoparticles: diagnostic magnetic resonance imaging and potential therapeutic applications in neurooncology and central nervous system inflammatory pathologies, a review. J Cereb Blood Flow Metab 30:15-35.

*P-Reviewer: You Q; C-Editors: Zhao M, Li CH; T-Editor: Jia Y*
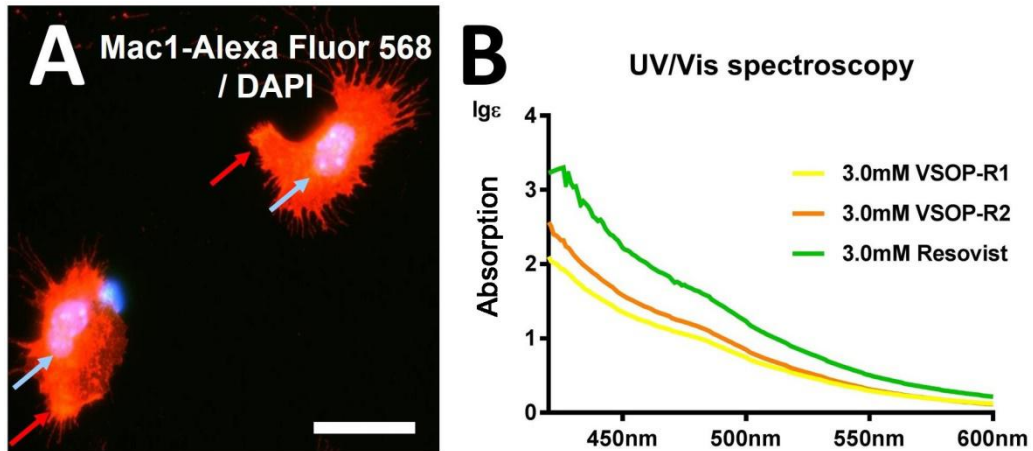
**Additional Figure 1 Monocyte morphology and SPIO absorption.**
(A) Fluorescence image of two isolated peripheral monocytes after 1 day *in vitro* showing characteristic kidney-shaped nuclei (light blue arrows, DAPI staining) as well as ubiquitous CD11b-receptor expression (red arrows, CD11b Alexa Fluor 568 labeling). Scale bar: 15 µm. (B) UV/Vis spectroscopy of VSOP-R1 (hydrodynamic diameter of 6.1 nm with 75% of particles within 4.1–7.5 nm), VSOP-R2 (hydrodynamic diameter of 8.7 nm with 75% of particles within 6.5–10.1 nm), and Resovist reflect differences in the SPIO absorption characteristics. CD11b: Cluster of differentiation molecule 11b; DAPI: 4',6-Diamidino-2-phenylindole; SPIO: superparamagnetic iron oxide nanoparticles; UV/Vis: ultraviolet-visible; VSOP: very small superparamagnetic iron oxide particles.